Influence of material migration on the mechanical integrity of inverted organic solar cells

Aurélien Tournebize, Dargie Deribew, Alberto Gregori, Roger C. Hiorns, Andreas Distler, Hans-Joachim Egelhaaf, Christine Lartigau-Dagron, Ahmed Allal, Agnès Rivaton, Heiko Peisert, et al.

Influence of material migration on the mechanical integrity of inverted organic solar cells

Aurélien Tournebize[1,4,5], Dargie Deribew[2], Alberto Gregori*[3], Roger C. Hiorns[3], Andreas Distler[2#], Hans-Joachim Egelhaaf[2#], Christine Lartigau-Dagron[3], Ahmed Allal[3], Agnès Rivaton[4,5], Heiko Peisert[1], and Thomas Chassé[1]

[1] Eberhard Karls Universität Tübingen, Institut für Physikalische und Theoretische Chemie, 72076 Tübingen, Germany

[2] OPVIUS GmbH (formerly Belectric OPV GmbH), Landgrabenstrasse 94, D-90443 Nürnberg, Germany

[3] CNRS/Univ Pau & Pays Adour, Institut des Science Analytiques et Physico-Chimie pour l'Environnement et les Materiaux, UMR 5254, 64000, Pau, France

[4] Université Blaise Pascal, Institut de Chimie de Clermont-Ferrand, Équipe Photochimie, BP 10448, F-63000 Clermont-Ferrand, France

[5] CNRS, UMR 6296, ICCF, Équipe Photochimie, BP 80026, F-63171 Aubière, France

* Communicating author: gregori.alberto@gmail.com

[#] Present address: Bavarian Center for Applied Energy Research, Solar Factory of the Future, Fürther Str. 250, D-90429 Nürnberg

Abstract

We have identified modifications of material distributions in inverted organic solar cell structures during accelerated aging processes that are potentially linked to the loss of the mechanical integrity of the devices. Non-encapsulated devices were treated with ISOS-D-3 ageing (the so called damp heat exposure at 85 °C/85% room humidity in the dark). After performing pull-off tests, the exposed surfaces were analyzed by X-ray photoemission spectroscopy and atomic force microscopy. For fresh devices, the results revealed that mechanical failure occurs close to the PEDOT:PSS/P3HT:PCBM interface, in agreement with the literature. However, after a short exposure to damp heat, XPS investigations indicate an enrichment of PCBM at the PEDOT:PSS/P3HT:PCBM interface and a change in the

PEDOT:PSS surface composition. Both phenomena may explain the rapid drop in device performances and the increased tendency towards delamination.

Keywords: Stability; ISOS-D3; delamination; PCBM diffusion

1. Introduction

Delamination is a known issue for organic solar cells [1,2]. The adhesion between several layers based on metals, and organic and inorganic materials is sensitive to mechanical deformation occurring during solar cell fabrication and the operating lifetime. Moreover, diffusion of water and oxygen [3] induces a material dependent degradation [4], which can furtherly undermine the device mechanical stability. Although device encapsulation strongly mitigate these effects [5], the evolution of the layers physico-chemical properties still plays a fundamental role in long-term device stability [6,7]. Poly(3,4-ethylenedioxythiophene) doped with poly(styrene sulfonate) (PEDOT:PSS), is one of the most widely used hole-transport materials in organic solar cells. In devices where hygroscopic PEDOT:PSS is used as hole transporting layer (HTL), a particular concern is the diffusion of water molecules resulting in a loss of photovoltaic properties and mechanical integrity [4]. This delamination of the PEDOT:PSS layer increases electrical resistance and affects the electric field distribution at the PEDOT:PSS/photo-active interface, resulting in a hindrance of charge extraction processes [3,8]. The subsequent deterioration of various PV parameters, in particular the fill factor (*FF*), can be observed from

the changes in the shape of the current density − voltage (*J*-*V*) curves. Specifically, changes occur in the values of the series (R_S) and shunt resistances (R_{SH}). A high R_S is expected to lower the *FF* and with it the maximum power point (V_{mpp}) of the cell.

Recently, we investigated the adhesive properties of non-encapsulated, inverted OSCs based on three different p-type polymers and two PEDOT:PSS formulations [9], using a controlled pull-off test. With any given combination of active layer and PEDOT:PSS formulation, the fracture plane was near the interface between the two. To gain insight into the adhesive failure and the effect of the manufacturing processes, Dupont *et al.* investigated the interlayer adhesion in inverted polymer solar cells with respect to the deposition technique be it spin, spray or slot-die coating, of the active layer [10,11]. They observed the same adhesive failure for all deposition techniques, located at the interface between the active layer (P3HT:PCBM) and the hole transporting layer (PEDOT:PSS), suggesting a material-dependent mechanism. Moreover, they investigated the influence of temperature, solar irradiation, and humidity on these properties. While the thermally induced changes in morphology, specifically vertical phase segregation, lead to an improved adhesion in the case of annealing [12] and solar irradiation, the combined effect of stress and humidity greatly accelerated the decohesion rate in the hygroscopic PEDOT:PSS layer through a moisture-assisted mechanism [13].

In the present work, we examine the change in materials composition at the weakest mechanical point of non-encapsulated inverted devices, degraded according to the ISOS-D-3 protocol [14], also known as damp-heat test (85 °C/85% relative humidity, rH, in the dark). The

layers were deposed by doctor blading on glass ITO, with the following layer stack ITO/ZnO/P3HT:$PC_{60}BM$/PEDOT:PSS/Ag, and Clevios^{TM} HTL Solar as PEDOT:PSS. The evolution of both electrical parameters and devices mechanical integrity was monitored by means of *JV* and pull-off test. The exposed surfaces were then analyzed by XPS and AFM respectively to obtain the chemical composition and the surface topography to identify the fracture plane.

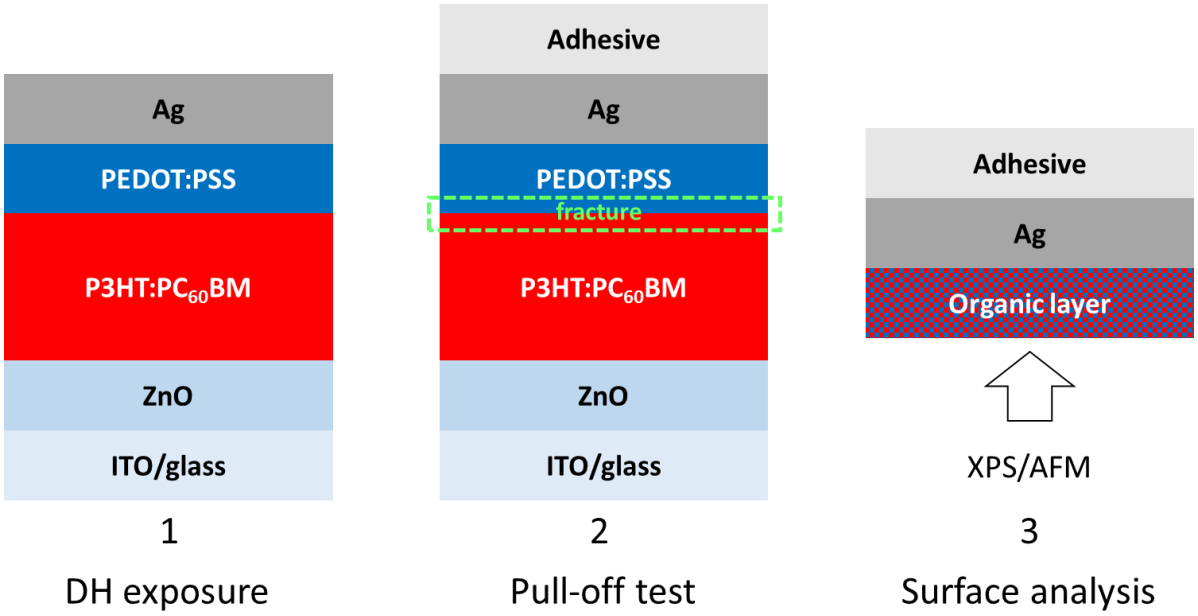

Figure 1. Experimental protocol including the exposure to damp heat (DH): Step 1: complete structure to monitor the electrical parameters; step 2: the pull-off test cracks the device and device is separated in upper and lower parts; Step 3: the upper parts were kept for XPS and AFM analyses.

2. Experimental

2.1. OSCs fabrication, characterization and degradation

Inverted devices with the structure glass/ITO/ZnO/P3HT:$PC_{60}BM$/PEDOT:PSS/Ag were fabricated using standard procedures. First, the glass/ITO substrates were cleaned in an ultrasonic bath of acetone and propan-2-ol for 10 min. Following cleaning, the substrates were dried and treated by UV-ozone for 10 min. A 5 wt% ZnO nanoparticle suspension in ethanol was coated on top of the cleaned glass/ITO substrate and then annealed in air at 140 °C for 10 min. The photoactive layer, 250 nm of P3HT:$PC_{60}BM$ obtained from using a 1:0.8 w/w solution in xylene:1-methylnaphthalene (7:1, v/v stirred overnight) coated on top of the ZnO layer. PEDOT:PSS (Clevios^{TM} HTL Solar) was coated directly from the commercial aqueous dispersion on top of the active layer. All layers were coated in air using a doctor blade. The devices were then completed by thermally evaporating 300 nm of Ag electrode on a customized mask. Before the evaporation of the metal electrode, the photoactive layer was annealed (N_2, 140 °C, 5 min). For degradation, devices were exposed to damp heat in a climate chamber (85 °C/85% humidity) for a specific period of time. For light current – voltage measurements, cells were illuminated with a simulated solar spectrum from Oriel solar simulator at 100 mW cm^{-2}. The *J-V* characteristics of the devices were recorded using a Keithley 2400 SMU in combination with a Keithley 7001 Multiplexer system and custom software.

2.2. Pull-off test

The use of the pull-off test for the characterization of the mechanical stability of OPV devices has been presented and thoroughly described in a previous publication [9]. For this set of experiments, we used a circular probe with a diameter of 12 mm. The epoxy adhesive

(SADER® from Bostik S. A.) was prepared before each measurement. The approaching speed of the probe was 50 μm s^{-1}, with a sampling frequency of 100 Hz. The force sensor used was a TME F108TC (1–100 N, ±0.05 N). The pulling speed was 10 μm s^{-1}, with a sampling frequency of 100 Hz. The pictures were taken with a Canon IXUS 132 and images were analyzed using ImageJ [15]. The test was performed on 5 different areas of samples fabricated on different substrates in the same batch, at different degradation stages (0, 0.5 and 8 h).

2.3. Surface analyses

XPS measurements were carried out using a multi-chamber UHV-system (base pressure 2 $x10^{-10}$ mbar), equipped with a SPECS Phoibos 150 cylindrical hemispherical analyser and a monochromatic Al Kα source (Focus 500 monochromator, XR50m X-ray source, hν(Al Kα) = 1486.74 eV). A Nanoscope IIIa atomic force microscope (AFM) from Veeco Instruments was used for surface topography measurements.

3. Results and discussion

3.1. Degradation and device performances

Inverted devices (glass/ITO/ZnO/P3HT:PC_{60}BM/PEDOT:PSS/Ag) were fabricated and immediately exposed to damp heat (85 °C/85% rH in the dark, ISOS-D3 [14]), while monitoring the evolution of the *J-V* curves and of the photovoltaic parameters with time (reported in Fig. 2).

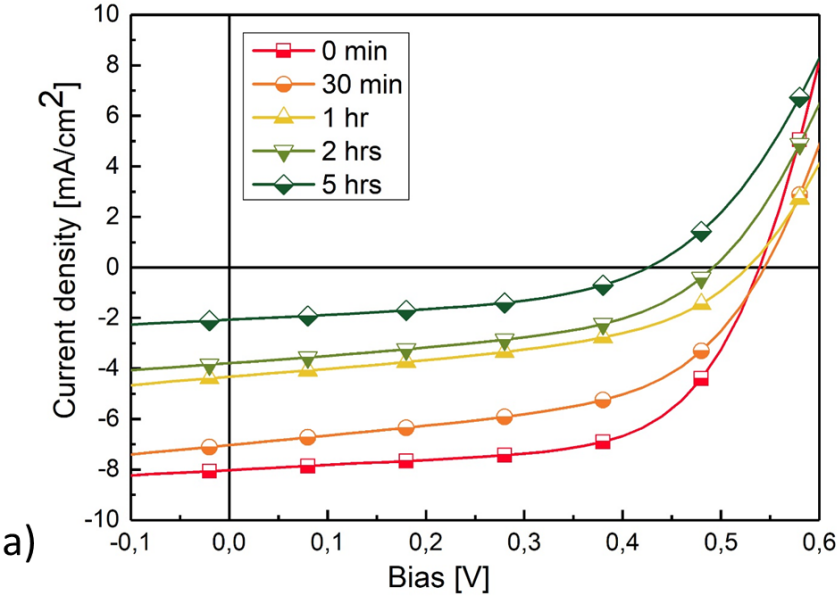
a)
0 min
30 min
1 hr
2 hrs
5 hrs
Current density [mA/cm2]
Bias [V]

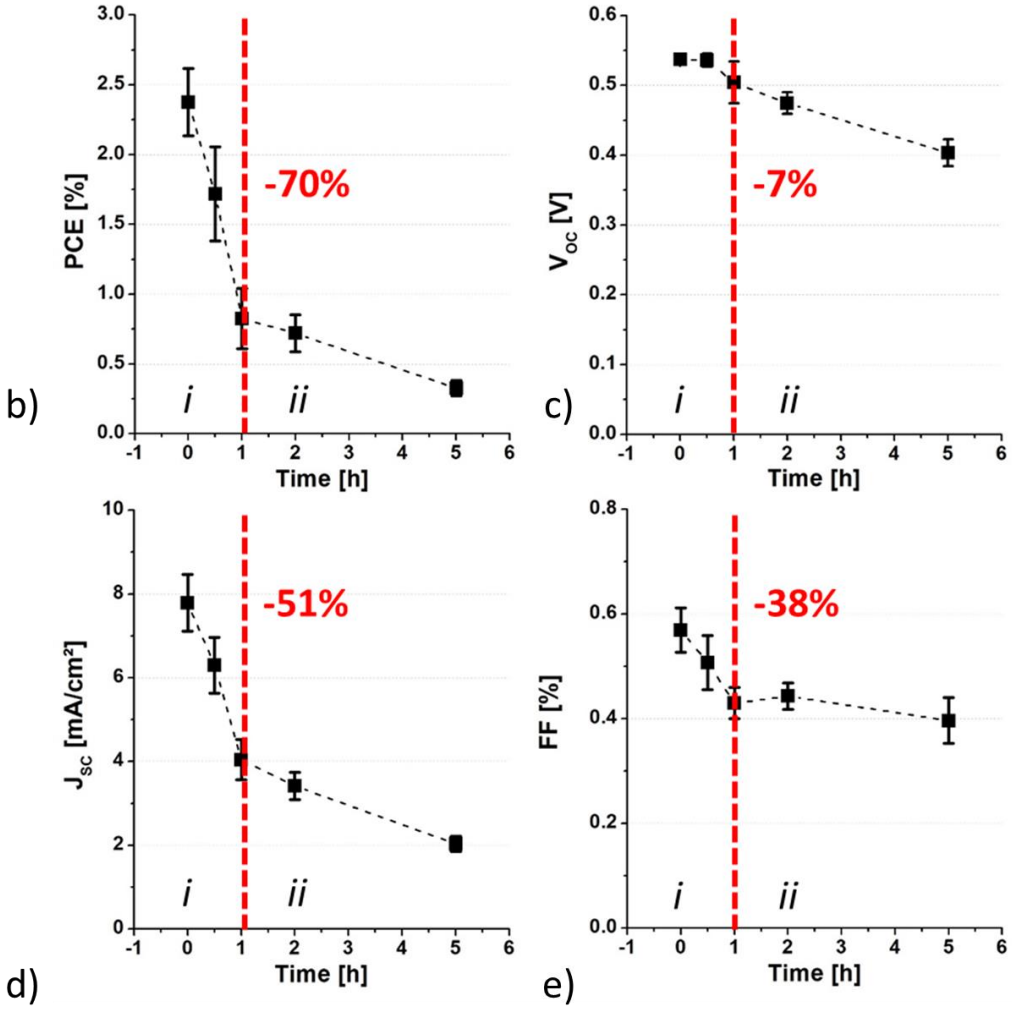
b)
PCE [%]
-70%
i
ii
Time [h]
c)
Voc [V]
-7%
i
ii
Time [h]
d)
Jsc [mA/cm²]
-51%
i
ii
Time [h]
e)
FF [%]
-38%
i
ii
Time [h]

Figure 2. Evolution of PV performance of solar cells of the architecture glass/ITO/ZnO/P3HT:$PC_{60}BM$/PEDOT:PSS/Ag during damp heat exposure (a) *JV* curves (b-e) photovoltaic parameters. A red dashed vertical line (t=1 h) acts as a guideline to show the two steps (i and ii) of degradation.

As the devices were not encapsulated, the damp heat exposure induced a rapid drop in device efficiencies. From Fig. 2 b-e), we can clearly distinguish two degradation steps:

i) A rapid loss of 70% of the PCE occurs during the first hour of DH exposure, due to a simultaneous decrease in J_{sc} (by 51%) and FF (by 38%), while V_{oc} remains relatively stable, showing a variation of around 7%.

ii) Subsequently, the degradation is driven by a loss of V_{oc} and mainly J_{sc}, while the FF is almost stable.

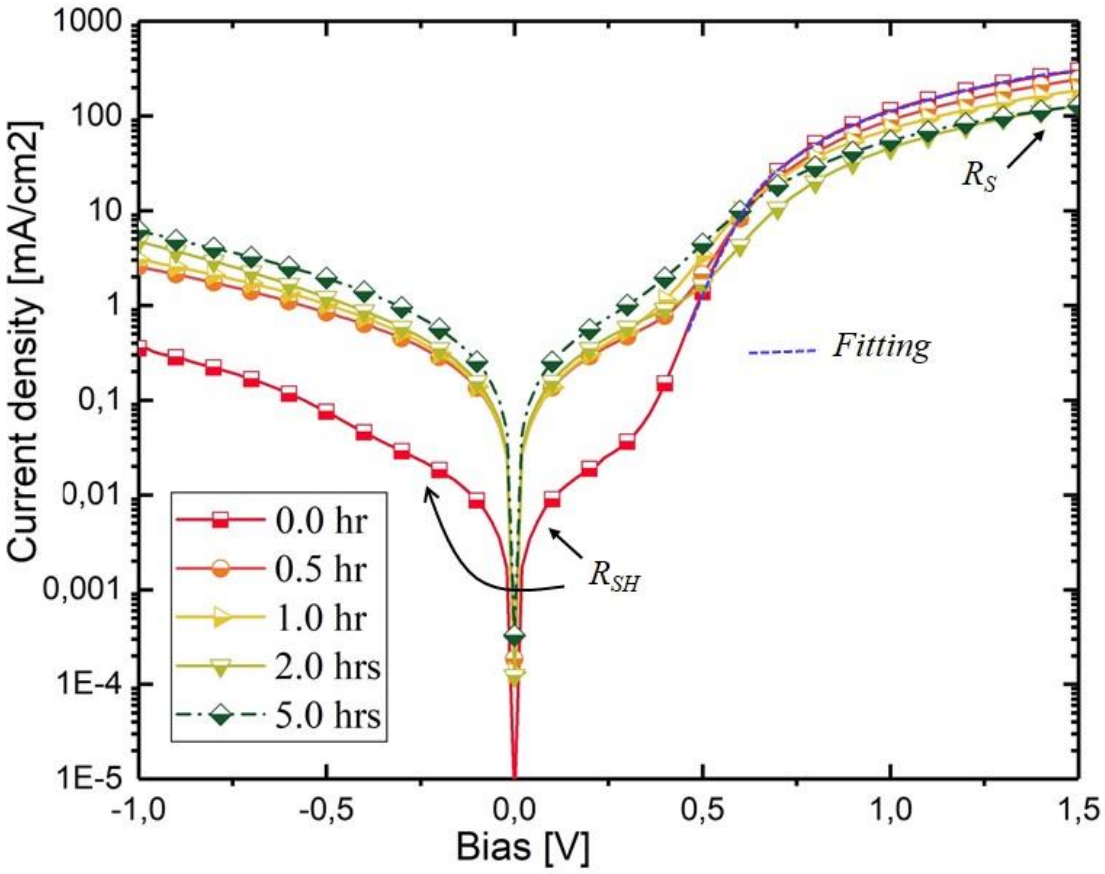

Figure 3. Dark JV curves of fresh and aged (damp heat, 85 °C/85% rH) solar cell devices.

Table 1. PV parameters of fresh and aged (damp heat, 85 °C/85% rH) solar cell devices (average values on 8-16 devices, according to the degradation stage).

Damp heat exposure time [h]	V_{OC} **[V]**	J_{SC} **[mA cm^{-2}]**	***FF*** **[%]**	**PCE [%]**	R_S **[Ω cm^2]**	R_{SH} **[kΩ cm^2]**
0	0.54 ± 0.01	7.8 ± 0.7	57.0 ± 4	2.4 ± 0.2	2.37 ± 0.01	11.4
0.5	0.54 ± 0.01	6.3 ± 0.7	51 ± 5	1.7 ± 0.3	2.74 ± 0.01	0.75
1.0	0.50 ± 0.03	4.0 ± 0.5	43 ± 3	0.8 ± 0.2	3.61 ± 0.02	0.34
2.0	0.48 ± 0.02	3.4 ± 0.3	44 ± 3	0.7 ± 0.1	4.79 ± 0.02	0.64
5.0	0.40 ± 0.02	2.0 ± 0.2	40 ± 4	0.33 ± 0.06	5.70 ± 0.01	0.40

Table 1 summarizes the evolution of the photovoltaic parameters and of the series (R_S) and shunt (R_{SH}) resistances. The approximate values of R_S and R_{SH} are extracted by fitting the semi-logarithmic dark-current density curves using the general equivalent circuit model for organic solar cells [16] (Fig. 3) at forward bias (i.e. near the saturation region) and at the ohmic part of the *J-V* curve (near the origin), respectively. R_S increases from 2.37 ± 0.01 Ω cm^2 of fresh devices to 5.70 ± 0.01 Ω cm^2 after 5 h of damp heat ageing, while R_{SH} decreases by one order of magnitude after only 0.5 h. This behavior is clearly visible in the *J-V* curves under illumination. It is well known that the fill factor, as well as the J_{SC}, are largely

influenced by series and parallel resistances [17]. Indeed, the FF decreases from an initial value of 57.0 ± 0.7 % to 43 ± 3 %, corresponding to a 25% reduction, after 1 h of ageing, while the J_{SC} drops by almost 50%, from 7.8 ± 0.7 to 4.0 ± 0.5 mA cm^{-2}. While the reduction in the V_{OC} is initially less pronounced (7% after 1 h), it accelerates in the second stage. The values obtained for the devices aged 8 h are not reported because they were, by that point, electrically dead.

3.2. Mechanical failure analysis

We followed the evolution of the device adhesive properties by means of the pull-off test. In Fig. 4, we report the stress at break values of fresh (0 h) and degraded (0.5 and 8 h) samples. We observe a slight drop (<22%) in the stress at break after 0.5 h and for longer times the value stays constant. The sensitivity of the measurement is also strongly affected; we attribute it to a water-based diffusion mechanism, which happens with an edge-to-center direction or through pin-holes [3,18], and leads to this wider range of values depending on the relative position of the tested area. Moreover, the relatively large size of the probe (1.1 cm^2) further contributes to this effect.

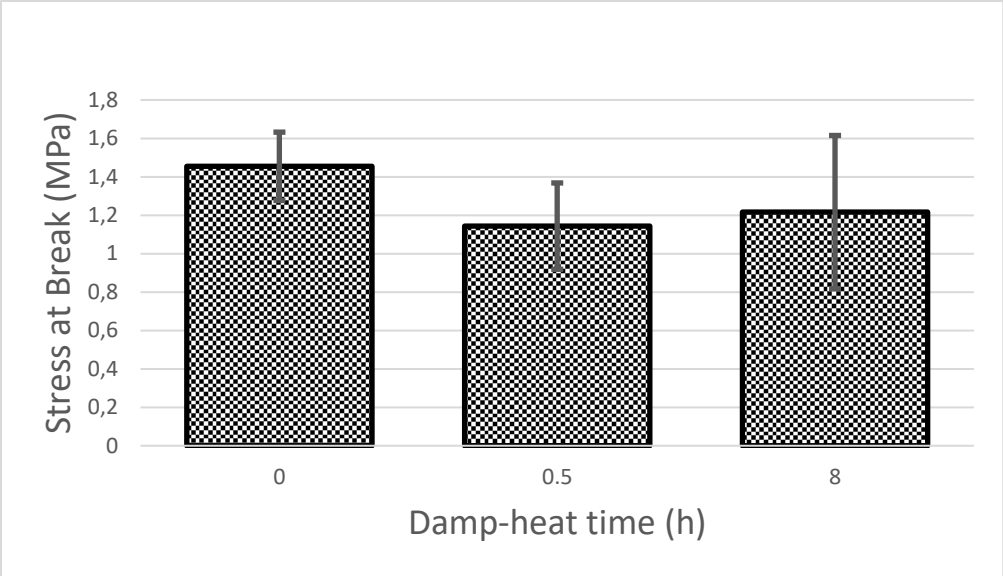

Figure 4. Evolution of the stress at break for fresh and degraded devices upon damp heat with time.

3.3. Identification of the fracture path

The pull-of test separates the devices in two parts, an upper and a lower, whose surfaces represent the weakest mechanical plane. The upper parts were subjected to XPS and AFM analyses to determine the atomic composition and the topography surface, respectively.

3.3.1. Fracture path of the fresh sample

In a prior work, we analyzed the fracture path of fresh devices with the same architecture by means of XPS [9]. The atomic composition observed in the lower part corresponded to a pure active layer of P3HT:$PC_{60}BM$, while the upper part was mainly composed of PEDOT:PSS, with a small contribution from the active-layer materials. Thus, the PEDOT:PSS/P3HT:$PC_{60}BM$ interface was interpreted as the mechanically weak point of the device, in agreement with previous results reported in the literature [11,19]. In the present study,

in good line with our prior work, the survey spectra of the fresh sample (Fig. 5, blue curve) is a combination of PEDOT:PSS with traces of P3HT:PCBM [9]. It should be noted though that the presence of silver from the top electrode is indicated.

3.3.2. Fracture path of the aged samples

In Fig. 5, we show the change in the XPS spectra, the atomic composition, with the corresponding photograph of the sample following damp heat (DH) exposure. Detailed data of atomic composition, obtained from the intensity of the respective core level spectra, are presented in Table 2. Upon visual inspection, we observed a yellowing of the sample surface with increasing DH exposure time. After 0.5 h and 8 h of DH exposure, the XPS data clearly show a carbon enrichment of the fracture surface, while the S2p decreases. This can be explained by the presence of active layer materials, especially PCBM. However, we can note that the relative oxygen content (9.9%) slightly increases up to 11.2% after 0.5h of DH exposure, which cannot be explained only by a PCBM enrichment. We will discuss this point later when considering the evolution of the S2p signal. To derive more information, it is necessary to analyze the core level signals in more detail.

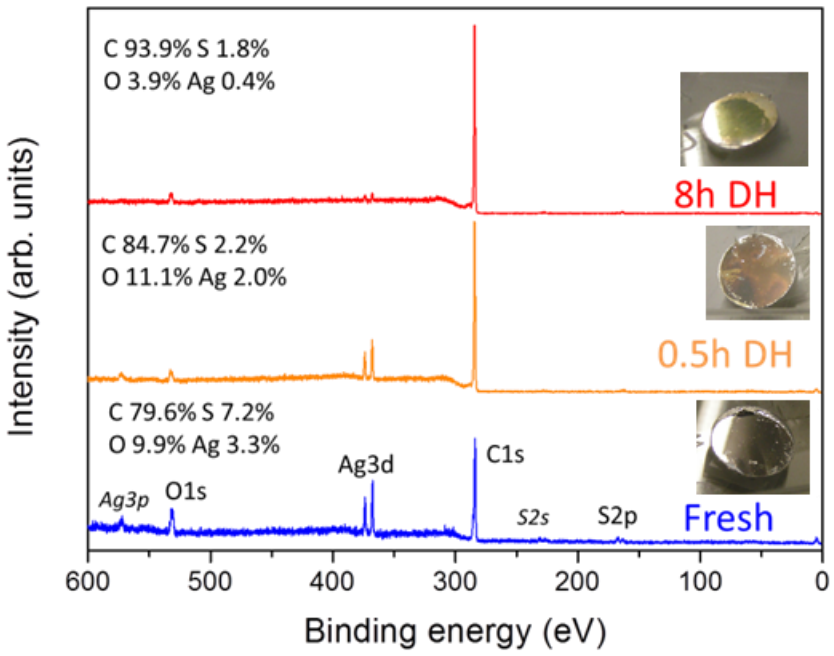

Figure 5. XPS survey spectra of the upper parts of fresh and degraded devices upon damp heat. Photographs and atomic compositions are reported as insets.

Table 2. Atomic composition of the upper part at different degradation stages (1-3) and the corresponding reference layers (4-7).

		C1s	S2p	O1s	Na1s	Ag3d	C/S	C/O
1	Fresh	79.6	7.2	9.9	-	3.3	11.0	8.0
2	0.5 h	84.7	2.2	11.2	-	2.0	38.5	7.6
3	8 h	93.9	1.8	3.9	-	0.4	52.2	24.1
4	PEDOT:PSS	69.5	6.0	24.0	0.5	-	11.6	2.9
5	P3HT:$PC_{60}BM$	90.7	6.9	2.4	-	-	13.1	37.8
6	P3HT	91.3	8.7	-	-	-	10.5	-
7	PCBM	90.9	-	9.1	-	-	-	10.0

Fig. 6 focuses on the C1s signals of fresh and 0.5 h aged samples, comparing them with, respectively, PEDOT:PSS and PCBM references. The main peak at ~284.5 eV in both cases is related to C-C bonds, whereas the high binding energy (BE) shoulder in the C1s spectrum of PEDOT:PSS is ascribed to C atoms in PEDOT, which are bonded to oxygen atoms. Thus, the height of this shoulder depends on both the PEDOT:PSS mixing ratio at the surface and the presence of additional carbon compounds. Features at BEs higher than 287 eV are ascribed to highly oxidized carbon species or so-called shake-up satellites.

In Fig. 6.a, we see that the signal for the upper part of the fresh sample shows the typical high BE shoulder of the PEDOT:PSS reference, although the relative intensity of this

component is weaker. After a 0.5 h DH exposure, the shoulder has almost disappeared, and the shape of the C1s signal is similar to that of the PCBM reference (Fig. 6.b). Also, signals at higher BE, typical for PCBM (arising from shake-up structures and the methyl ester group) become visible. Thus, we conclude that PCBM molecules diffuse toward the active layer/HTL interface as a consequence of the damp-heat treatment.

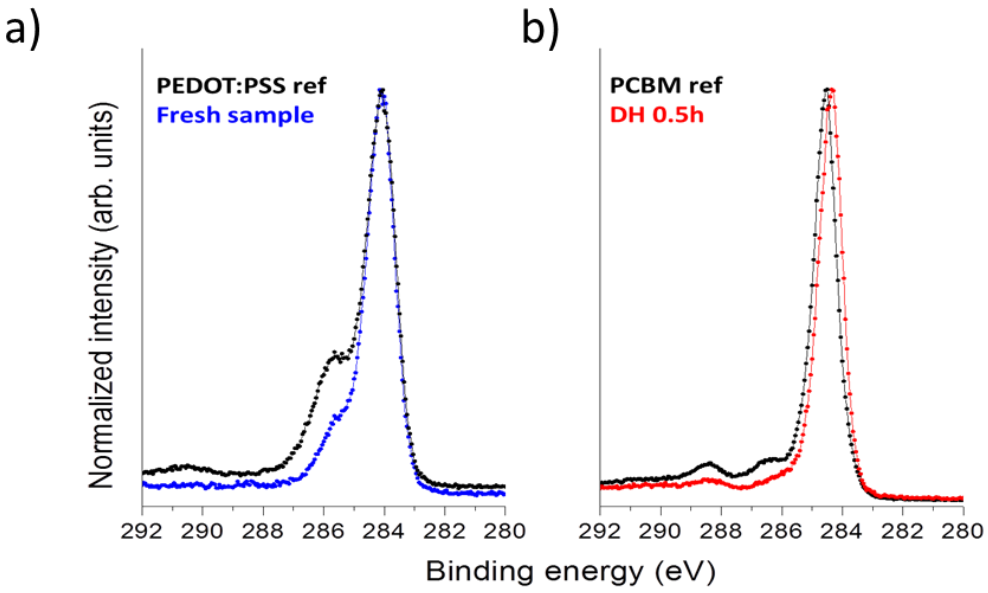

Figure 6. a) C1s signals of the fresh delaminated sample (blue) and PEDOT:PSS as reference (black); b) C1s signals of the upper part after 0.5 h DH (red) and PCBM as reference (black).

The question arises, if the PEDOT:PSS mixing ratio is also changed at the active layer/PEDOT:PSS interface. In Fig. 7.a, we compare the S2p signal of the fresh sample to the one of the 0.5 h DH. We notice that the fresh one is quite similar to the PEDOT:PSS, with an approximate 2:1 ratio between PSS and PEDOT, with an additional feature at low binding energy. An $S2p_{3/2}$ signal at 161.1 eV corresponds to metal sulfide [20], such as Ag_2S [21], meaning that Ag has diffused from the electrode into the PEDOT:PSS layer [22]. In order to

confirm this, we performed a fitting of the S2p signal (Fig. 7.b). It shows that the upper part of the fresh sample is mainly composed of PEDOT:PSS, with a small contribution of Ag_2S. After 0.5 h of DH exposure, the S2p signal becomes very noisy due to the low amount of sulfur (2.2%), caused by carbon enrichment. However, some intensity in the range of PEDOT/P3HT-S2p (162-165 eV) and Ag_2S (161 eV) is visible, whereas the PSS-S2p signal at 167-169 eV is below the detection limit. This finding can be explained either by a PEDOT enrichment or by traces of P3HT [23] at the fracture plane. The change in atomic composition (Table 2) suggests that the first explanation is more likely. Indeed, we have observed a slight increase of relative oxygen content after a 0.5h of DH exposure that cannot be consistent with a P3HT enrichment (P3HT bears no oxygen atoms while PEDOT has 11.1% of oxygen atoms). Figure S1 shows the O1s signal of the fresh and 0.5h exposed samples. For the fresh sample, the two signals can be assigned to the oxygen belonging to PEDOT (531.8 eV) and PSS (530.6 eV). After 0.5h of DH exposure, we observe an almost complete disappearance of the PSS-related shoulde at the low binding energy. On the other hand, the enhanced intensity at the high binding energy side of the peak (> ~532 eV) may be assigned to additional adsorbed water on the polymer surface. The presence of doped P3HT is unlikely as p-doping of P3HT requires the combined oxygen and light exposure, which is not the case here [23].

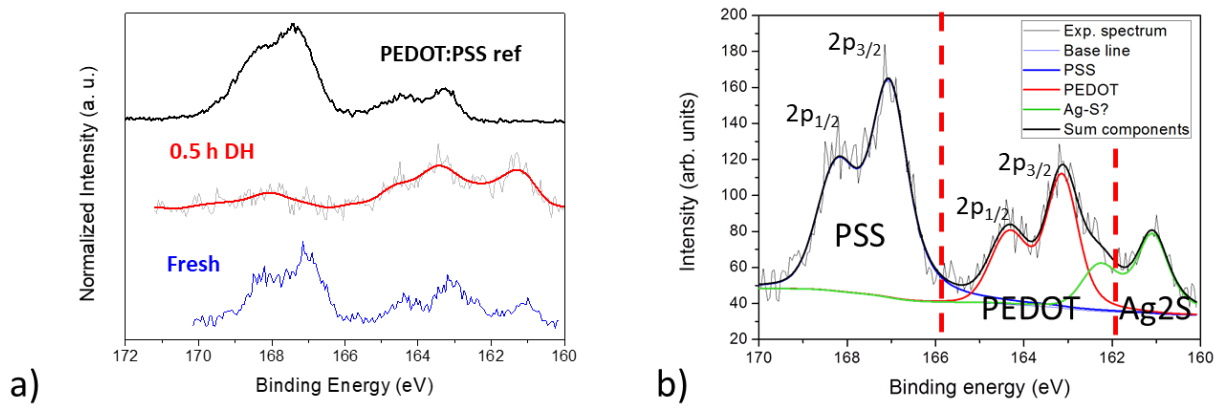

Figure 7. a) S2p signal of the fresh and 0.5 h DH exposed samples compared to PEDOT:PSS reference; b) peak deconvolution of S2p-fresh sample spectra, with contribution from PSS (blue), PEDOT (red) and Ag-S (green).

We also performed a topographic survey of the exposed surface by AFM (Fig. 8). The surfaces are all quite flat, with no particular features except for the upper part after 8 h of DH. Indeed, in the top right corner of the 20x20 μm image, some structures, possibly PCBM crystallites [24], are visible. Despite this and the chemical composition change, the surface roughness, expressed by the root mean square (RMS), slightly changes from 15.7 nm (0 h) to 14.3 nm (0.5 h), to the final value of 19.6 nm (8 h).

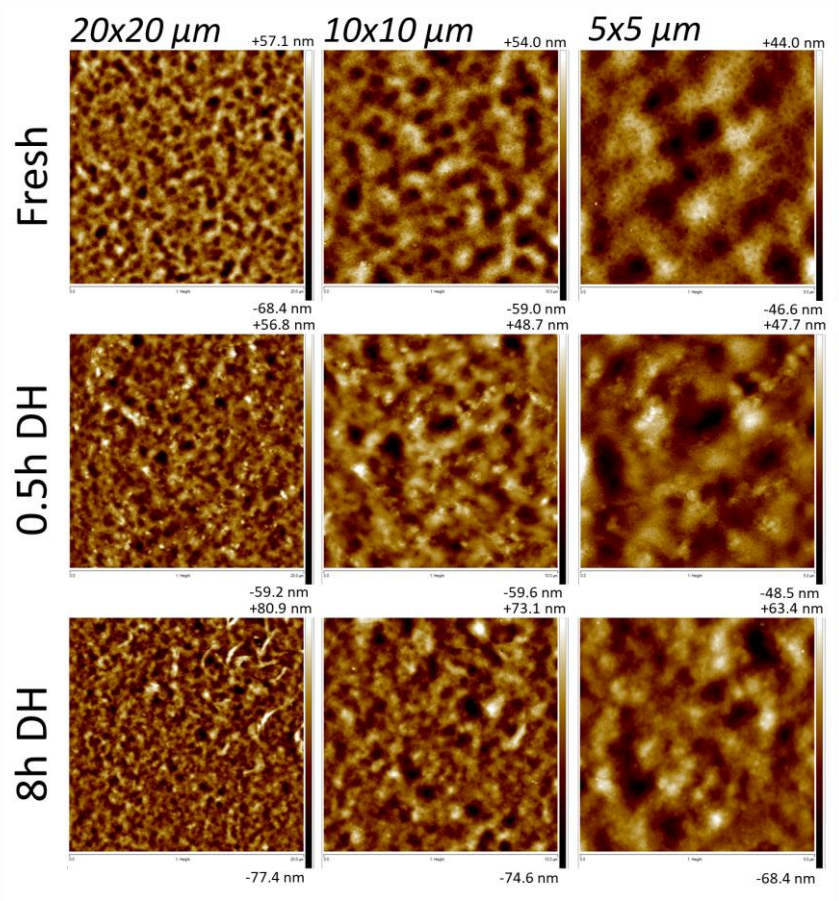

Figure 8. AFM topographic images of fresh and DH exposed upper parts at different scales: 20x20 µm, 10x10 µm, and 5x5 µm.

3.4. Tentative degradation mechanism

The rapid loss in stage i) is the result of materials migration at the HTL/active layer interface, while in stage ii) H_2O becomes predominant with a stronger reduction of V_{OC}, caused by a mismatch in the work function of the electrodes [25], and a further, slower reduction in J_{SC}. This two-stage mechanism is due to the experimental conditions, in particular to our choice of performing the damp heat test on non-encapsulated devices. Since the OSCs were not

exposed to light, we consider that oxidation (irreversible degradation) and p-doping (reversible degradation) are non-dominant degradation mechanisms compared to the moisture effect. We have observed that a DH exposure induces a rapid loss of device performances concomitant with a loss of mechanical integrity. Focusing on the 0.5 h exposure, the PCE and stress at break decreases of 27 and 22%, respectively. We propose a tentative mechanism to explain the loss of performance and mechanical integrity after such a short exposure. Through the XPS analysis of the fracture surface of fresh samples, we observe the expected PEDOT:PSS finger print, with traces of active layer and the presence of silver/silver-sulfur complexes. A short DH exposure 0.5 h leads to a drastic modification of the fracture plan, which is richer in $PC_{60}BM$ and poorer in PSS.

Balcaen *et al.* [12] observed an increase in adhesive energy of encapsulated devices under thermal stress, due to the formation of a PEDOT/P3HT intermixed layer. Dupont *et al.* [13] observed that the cohesion rate of the PEDOT:PSS layer is dependent on the synergistic effect of relative humidity, temperature, and mechanical stress. In our experiment, the devices were neither encapsulated nor underwent mechanical stresses. The different testing techniques (pull off *vs.* cantilever beam) and conditions (85°C/85% rH *vs*. thermal cycling or temperature/humidity/mechanical stresses) make it harder to compare our results. Under the described experimental condition, we did not assist to the formation of an intermixed interfacial layer [26] (and corresponding increased adhesion), but to the PCBM diffusion toward the AL/HTL interface. The thermally activated Oswalt ripening [27,28] depends on PCBM

diffusion and eventually leads to the formation of large aggregates [29], as we observed in the AFM images (Fig. 8). A thin layer of PCBM explains the yellowing, and contributes, through the corresponding evolution of the BHJ vertical phase segregation, to both the current density and the mechanical integrity losses. These findings are in good agreement with previous work [5,30], where a similar evolution of phase segregation and PV properties was observed for both encapsulated and non-encapsulated devices.

The presence of small molecules ($PC_{60}BM$) at a polymer/polymer interface may contribute to the loss of adhesion, reducing possible interchain interdigitation and charge transfer/coordination complex between PEDOT:PSS and P3HT [19]. The migration of PCBM towards the interface and the consequent phase separation account for the increase in R_S, while the decrease in R_{SH} is most probably due to the diffusion of Ag inside the layer stack [7].

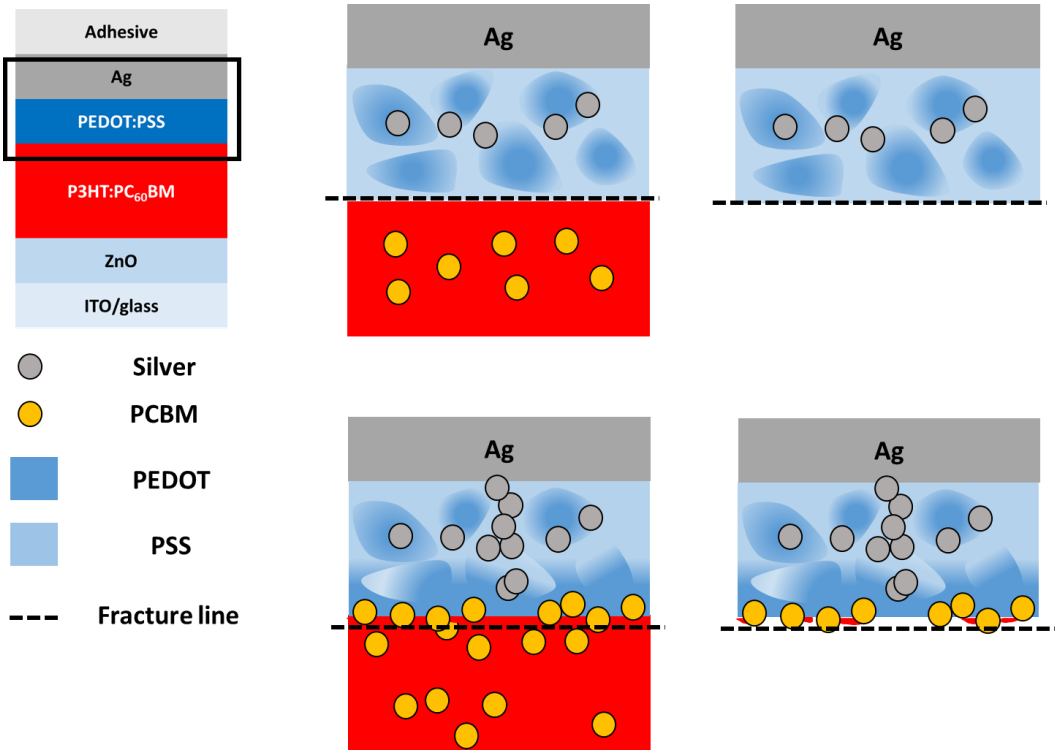

Figure 9. Proposed mechanism of delamination in inverted devices based on P3HT:$PC_{60}BM$/PEDOT:PSS exposed to damp heat.

4. Conclusion

Exposure to damp heat (85 °C/85% rH in the dark) of non-encapsulated solar cell devices has led to a drastic degradation of performances. Pull-off tests on fresh and degraded devices always showed a breaking point near the PEDOT:PSS/P3HT:PCBM interface. The aged samples, however, showed reduced adhesion strength and an enrichment of PCBM at the breaking point. Moreover, the interfacial composition of PEDOT:PSS layer changed in terms of an enhanced PEDOT to PSS ratio. These observations are assumed to be the reason behind an increased tendency towards delamination as well as a rapid device performance loss under these conditions.

Acknowledgements

The research leading to these results has received funding from the European Union Seventh Framework Program (FP7/2011) under grant agreement ESTABLIS no. 290022.

References

[1] M. Jørgensen, K. Norrman, S. a. Gevorgyan, T. Tromholt, B. Andreasen, F.C. Krebs, Stability of polymer solar cells, Adv. Mater. 24 (2012) 580–612. doi:10.1002/adma.201104187.

[2] M.T. Lloyd, C.H. Peters, A. Garcia, I. V. Kauvar, J.J. Berry, M.O. Reese, M.D. McGehee, D.S. Ginley, D.C. Olson, Influence of the hole-transport layer on the initial behavior and lifetime of inverted organic photovoltaics, Sol. Energy Mater. Sol. Cells. 95 (2011) 1382–1388. doi:10.1016/j.solmat.2010.12.036.

[3] J. Adams, M. Salvador, L. Lucera, S. Langner, G.D. Spyropoulos, F.W. Fecher, M.M. Voigt, S.A. Dowland, A. Osvet, H.J. Egelhaaf, C.J. Brabec, Water ingress in encapsulated inverted organic solar cells: Correlating infrared imaging and photovoltaic performance, Adv. Energy Mater. 5 (2015) 1–11. doi:10.1002/aenm.201501065.

[4] N. Grossiord, J.M. Kroon, R. Andriessen, P.W.M. Blom, Degradation mechanisms in organic photovoltaic devices, Org. Electron. 13 (2012) 432–456. doi:10.1016/j.orgel.2011.11.027.

[5] S.H. Kim, H.J. Son, S.H. Park, J.S. Hahn, D.H. Kim, A study for degradation of flexible organic photovoltaic modules via damp-heat test: By accessing individual layers of the module, Sol. Energy Mater. Sol. Cells. 144 (2016) 187–193. doi:10.1016/j.solmat.2015.08.037.

[6] S.B. Sapkota, A. Spies, B. Zimmermann, I. Dürr, U. Würfel, Promising long-term stability of encapsulated ITO-free bulk-heterojunction organic solar cells under different aging conditions, Sol. Energy Mater. Sol. Cells. 130 (2014) 144–150. doi:10.1016/j.solmat.2014.07.004.

[7] V.I. Madogni, B. Kounouhéwa, A. Akpo, M. Agbomahéna, S.A. Hounkpatin, C.N. Awanou, Comparison of degradation mechanisms in organic photovoltaic devices upon exposure to a temperate and a subequatorial climate, Chem. Phys. Lett. 640 (2015) 201–214. doi:10.1016/j.cplett.2015.09.023.

[8] K. Kawano, R. Pacios, D. Poplavskyy, J. Nelson, D.D.C. Bradley, J.R. Durrant, Degradation of organic solar cells due to air exposure, Sol. Energy Mater. Sol. Cells. 90 (2006) 3520–3530. doi:10.1016/j.solmat.2006.06.041.

[9] A. Gregori, A. Tournebize, S. Schumann, H. Peisert, R.C. Hiorns, T. Chassé, C. Lartigau-Dagron, A. Allal, The role of donor polymer and PEDOT:PSS formulation on adhesion processes in inverted organic solar cells, Sol. Energy Mater. Sol. Cells. 174 (2018). doi:10.1016/j.solmat.2017.08.024.

[10] S.R. Dupont, E. Voroshazi, P. Heremans, R.H. Dauskardt, The effect of anneal, solar irradiation and humidity on the adhesion/cohesion properties of P3HT:PCBM based inverted polymer solar cells, in: 2012: pp. 003259–003262. doi:10.1109/PVSC.2012.6318272.

[11] S.R. Dupont, M. Oliver, F.C. Krebs, R.H. Dauskardt, Interlayer adhesion in roll-to-roll processed flexible inverted polymer solar cells, Sol. Energy Mater. Sol. Cells. 97

(2012) 171–175. doi:10.1016/j.solmat.2011.10.012.

[12] V. Balcaen, N. Rolston, S.R. Dupont, E. Voroshazi, R.H. Dauskardt, Thermal cycling effect on mechanical integrity of inverted polymer solar cells, Sol. Energy Mater. Sol. Cells. 143 (2015) 418–420.

[13] S.R. Dupont, F. Novoa, E. Voroshazi, R.H. Dauskardt, Decohesion Kinetics of PEDOT:PSS Conducting Polymer Films, Adv. Funct. Mater. (2013) 1–8. doi:10.1002/adfm.201302174.

[14] M.O. Reese, S.A. Gevorgyan, M. Jørgensen, E. Bundgaard, S.R. Kurtz, D.S. Ginley, D.C. Olson, M.T. Lloyd, P. Morvillo, E.A. Katz, A. Elschner, O. Haillant, T.R. Currier, V. Shrotriya, M. Hermenau, M. Riede, K.R. Kirov, G. Trimmel, T. Rath, O. Inganäs, F. Zhang, M. Andersson, K. Tvingstedt, M. Lira-Cantu, D. Laird, C. McGuiness, S. Gowrisanker, M. Pannone, M. Xiao, J. Hauch, R. Steim, D.M. Delongchamp, R. Rösch, H. Hoppe, N. Espinosa, A. Urbina, G. Yaman-Uzunoglu, J.B. Bonekamp, A.J.J.M. Van Breemen, C. Girotto, E. Voroshazi, F.C. Krebs, Consensus stability testing protocols for organic photovoltaic materials and devices, Sol. Energy Mater. Sol. Cells. 95 (2011) 1253–1267. doi:10.1016/j.solmat.2011.01.036.

[15] National Institutes of Health, Open Source under Title 17, Sect. 105 USA Code. (n.d.).

[16] J.H. Lee, S. Cho, A. Roy, H.-T. Jung, A.J. Heeger, Enhanced diode characteristics of organic solar cells using titanium suboxide electron transport layer, Appl. Phys. A. 96 (2010) 163303. doi:10.1063/1.3409116.

[17] D. Gupta, M. Bag, K.S. Narayan, Correlating reduced fill factor in polymer solar cells to contact effects, Appl. Phys. Lett. 92 (2008) 2007–2009. doi:10.1063/1.2841062.

[18] K. Feron, T.J. Nagle, L.J. Rozanski, B.B. Gong, C.J. Fell, Spatially resolved photocurrent measurements of organic solar cells: Tracking water ingress at edges and pinholes, Sol. Energy Mater. Sol. Cells. 109 (2013) 169–177. doi:10.1016/j.solmat.2012.10.027.

[19] S.R. Dupont, E. Voroshazi, P. Heremans, R.H. Dauskardt, Adhesion properties of inverted polymer solarcells: Processing and film structure parameters, Org. Electron. Physics, Mater. Appl. 14 (2013) 1262–1270. doi:10.1016/j.orgel.2013.02.022.

[20] R.S.C. Smart, W.M. Skinner, A.R. Gerson, XPS of Sulphide Mineral Surfaces : Metal-deficient , Polysulphides , Defects and Elemental Sulphur, Surf. Interface Anal. 28 (1999) 101–105. doi:10.1002/(SICI)1096-9918(199908)28:1<101::AID-SIA627>3.0.CO;2-0.

[21] H. Jain, A. Kovalskiy, A. Miller, An XPS study of the early stages of silver photodiffusion in Ag/a-As2S3 films, J. Non. Cryst. Solids. 352 (2006) 562–566. doi:10.1016/j.jnoncrysol.2005.11.044.

[22] R. Rösch, D.M. Tanenbaum, M. Jørgensen, M. Seeland, M. Bärenklau, M. Hermenau, E. Voroshazi, M.T. Lloyd, Y. Galagan, B. Zimmermann, U. Würfel, M. Hösel, H.F. Dam, S.A. Gevorgyan, S. Kudret, W. Maes, L. Lutsen, D. Vanderzande, R. Andriessen, G. Teran-Escobar, M. Lira-Cantu, A. Rivaton, G.Y. Uzunoğlu, D. Germack, B. Andreasen, M. V. Madsen, K. Norrman, H. Hoppe, F.C. Krebs, Investigation of the degradation mechanisms of a variety of organic photovoltaic devices by combination of

imaging techniques - The ISOS-3 inter-laboratory collaboration, Energy Environ. Sci. 5 (2012) 6521–6540. doi:10.1039/c2ee03508a.

[23] H. Hintz, H. Peisert, H. Egelhaaf, T. Chass, Reversible and Irreversible Light-Induced p-Doping of P3HT by Oxygen Studied by Photoelectron Spectroscopy (XPS / UPS), (2011) 13373–13376.

[24] M. Campoy-Quiles, T. Ferenczi, T. Agostinelli, P.G. Etchegoin, Y. Kim, T.D. Anthopoulos, P.N. Stavrinou, D.D.C. Bradley, J. Nelson, Morphology evolution via self-organization and lateral and vertical diffusion in polymer:fullerene solar cell blends., Nat. Mater. 7 (2008) 158–164. doi:10.1038/nmat2102.

[25] C.J. Brabec, A. Cravino, D. Meissner, N. Serdar Sariciftci, T. Fromherz, M.T. Rispens, L. Sanchez, J.C. Hummelen, Origin of the open circuit voltage of plastic solar cells, Adv. Funtional Mater. 11 (2001) 374–380. doi:10.1002/1616-3028(200110)11:5<374::AID-ADFM374>3.0.CO;2-W.

[26] C. Bruner, F. Novoa, S. Dupont, R. Dauskardt, Decohesion Kinetics in Polymer Organic Solar Cells, (2014).

[27] S. Kouijzer, J.J. Michels, M. Van Den Berg, V.S. Gevaerts, M. Turbiez, M.M. Wienk, R.A.J. Janssen, Predicting morphologies of solution processed polymer:Fullerene blends, J. Am. Chem. Soc. 135 (2013) 12057–12067. doi:10.1021/ja405493j.

[28] N.D. Treat, M.A. Brady, G. Smith, M.F. Toney, E.J. Kramer, C.J. Hawker, M.L. Chabinyc, Interdiffusion of PCBM and P3HT reveals miscibility in a photovoltaically active blend, Adv. Energy Mater. 1 (2011) 82–89. doi:10.1002/aenm.201000023.

[29] G.E. Morse, A. Tournebize, A. Rivaton, T. Chassé, C. Taviot-gueho, N. Blouin, O.R. Lozman, S. Tierney, The effect of polymer solubilizing side-chains on solar cell stability, Phys. Chem. Chem. Phys. 17 (2015) 11884–11897. doi:10.1039/C5CP01158B.

[30] K. Norrman, M. V. Madsen, S. a. Gevorgyan, F.C. Krebs, Degradation Patterns in Water and Oxygen of an Inverted Polymer Solar Cell, J. Am. Chem. Soc. 132 (2010) 16883–16892. doi:10.1021/ja106299g.

Appendix A: Supporting Information

Influence of material migration on the mechanical integrity of inverted organic solar cells

Aurélien Tournebize[1,4,5], Dargie Deribew[2], Alberto Gregori*[3], Roger C. Hiorns[3], Andreas Distler[2#], Hans-Joachim Egelhaaf[2#], Christine Lartigau-Dagron[3], Ahmed Allal[3], Agnès Rivaton,[4,5] Heiko Peisert[1], and Thomas Chassé[1]

[1] Eberhard Karls Universität Tübingen, Institut für Physikalische und Theoretische Chemie, 72076 Tübingen, Germany

[2] OPVIUS GmbH (formerly Belectric OPV GmbH), Landgrabenstrasse 94, D-90443 Nürnberg, Germany

[3] CNRS/Univ Pau & Pays Adour, Institut des Science Analytiques et Physico-Chimie pour l'Environnement et les Materiaux, UMR 5254, 64000, Pau, France

[4] Université Blaise Pascal, Institut de Chimie de Clermont-Ferrand, Équipe Photochimie, BP 10448, F-63000 Clermont-Ferrand, France

[5] CNRS, UMR 6296, ICCF, Équipe Photochimie, BP 80026, F-63171 Aubière, France

[#] Present address: Bavarian Center for Applied Energy Research, Solar Factory of the Future, Fürther Str. 250, D-90429 Nürnberg

CONTENTS

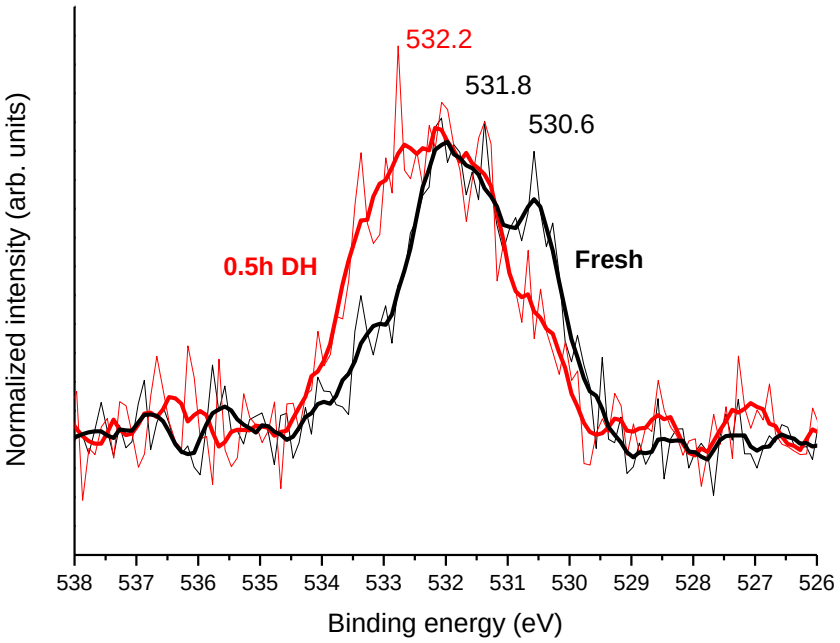

Figure S1. Normalized XPS spectra in the O1s region of the fresh and 0.5h DH delaminated samples.